Cell Reports, Volume *35*

Supplemental information

Differential effect of sleep deprivation on place cell representations, sleep architecture, and memory in young and old mice

Robin K. Yuan, Matthew R. Lopez, Manuel-Miguel Ramos-Alvarez, Marc E. Normandin, Arthur S. Thomas, David S. Uygun, Vanessa R. Cerda, Amandine E. Grenier, Matthew T. Wood, Celia M. Gagliardi, Herminio Guajardo, and Isabel A. Muzzio

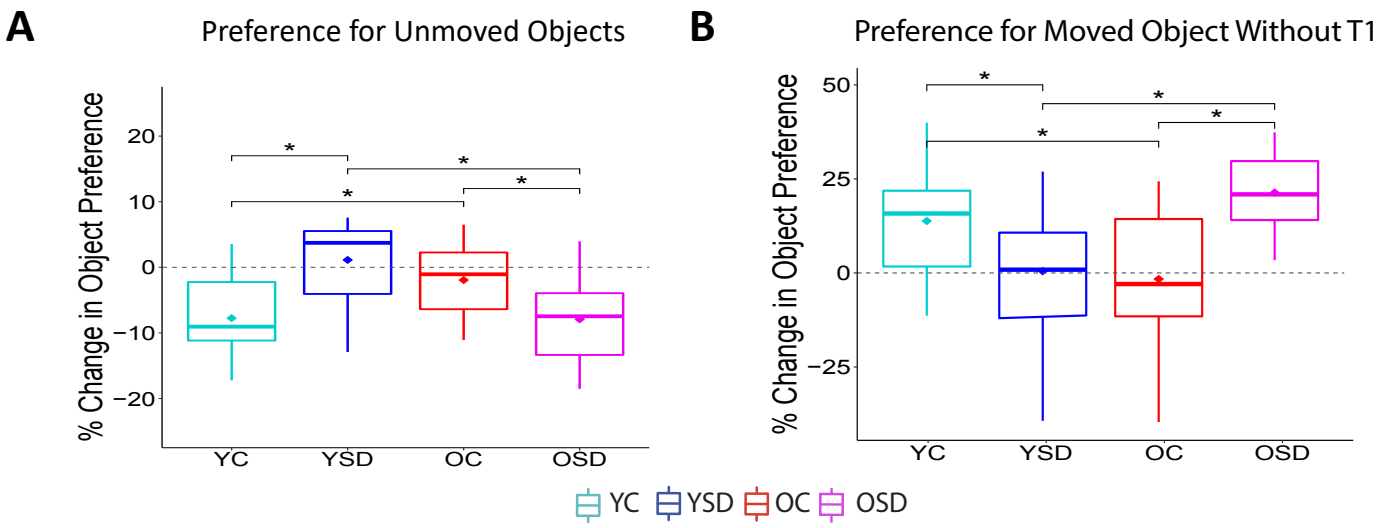

Figure **1S, related to Figure 1**. Preference for unmoved objects and preference for moved object without including trial 1. A. The percent change in preference for the unmoved objects showed an interaction between age and sleep condition [Fw(1)=0.55, p<0.0001. Single effects corroborated that young controls and old SD mice displayed less preference for the unmoved objects [YC vs. YSD: Tw(16.07)=11.51, p<0.01, OC vs. OSD: Tw(15.10)=4.47, p<0.05], but there were no significant differences between the young SD and old controls [YSD vs. OC: Tw(15.58)=1.30, p=0.26], indicating that poor OPR performance in these groups was not due to a shift in preference for unmoved objects. B. Percent change in object preference excluding the first object trial to ensure that the results were not biased by a possible novelty effect during the first object exposure. Results were almost identical to those including all trials [interaction age vs. sleep: Fw(1):0.55, p<0.0001, YC vs. YSD: Tw(17.06)=2.15,p<0.05; OV vs. OSD: Tw(13.66)=3.74, p<0.003; YC vs. OC: Tw(16.13)=2.34, p<0.04, YSD vs. OSD: Tw(14.50)=3.66, p<0.003**E**], indicating that the observed differences were not due to variability in object exploration.

Figure 1S

Electrode placements and place cell parameters

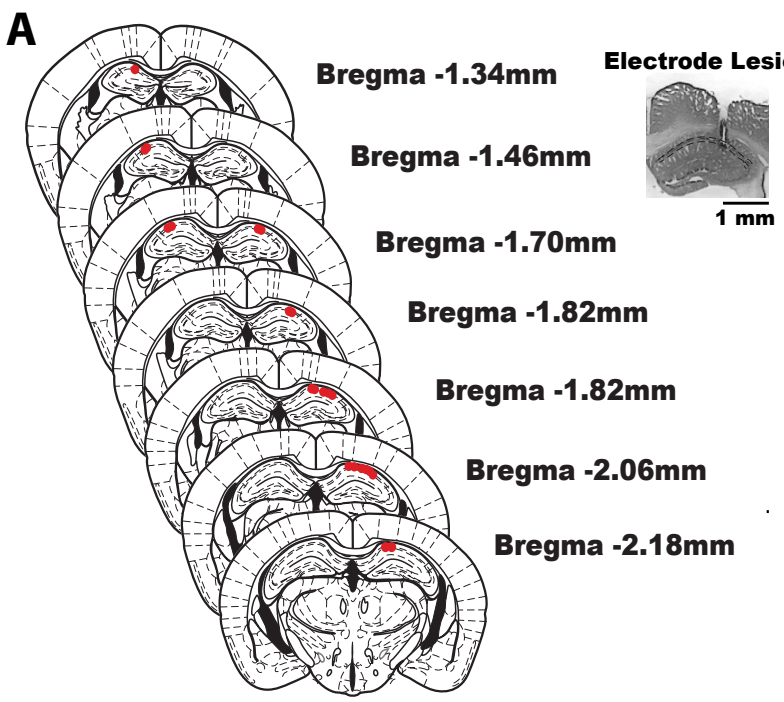

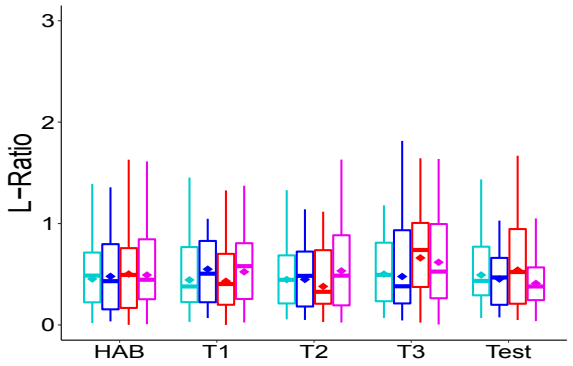

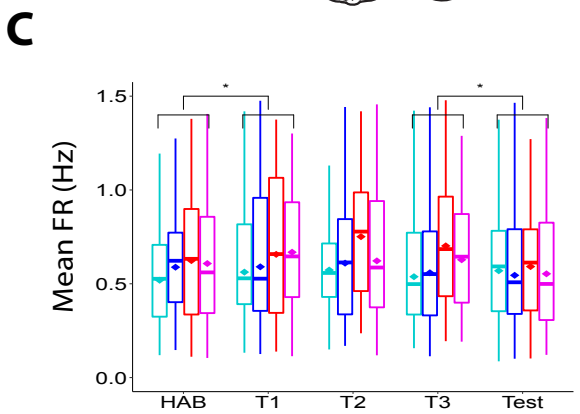

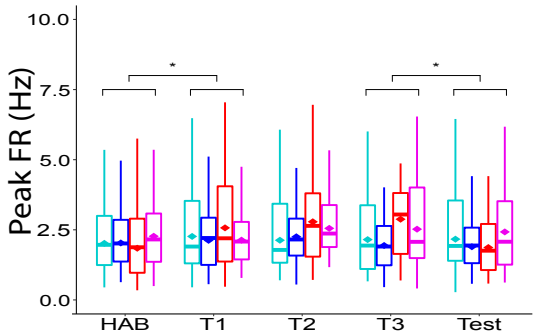

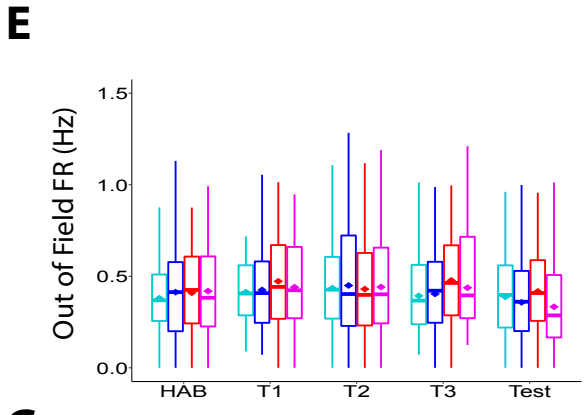

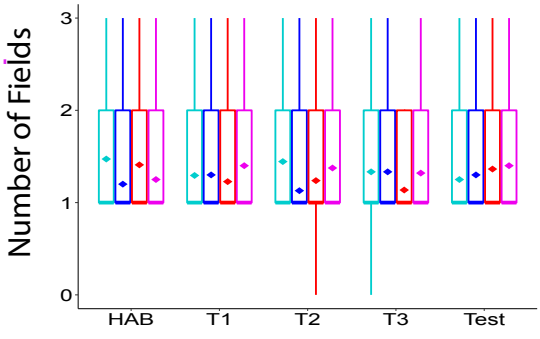

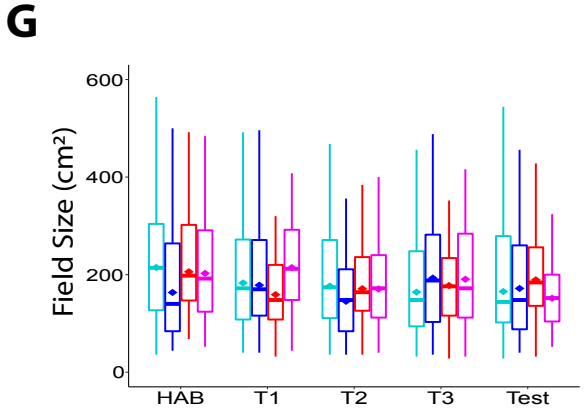

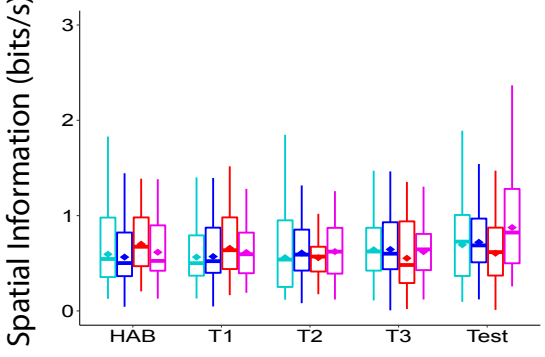

Figure S2

Figure S2, related to Figure 2. . Electrode placements and place cell parameters. A) Schematic of electrode placements (red dots) and microphotograph showing sample lesion marking electrode placement in CA1, scale bar represents 1 mm. B) Cluster L-ratio for all groups across trials. C-E) Mean (C), peak (D), and out of field (E) firing rate for all groups across trials. There were no differences in mean or peak firing rate between the groups throughout training ($p>0.05$). However, there were increases in firing rate that persisted during training (T1 to T3) when the objects were introduced across all groups [MFR: $Fw(4)=1.14$, $p<0.007$; PFR: $Fw(4)=1.11$, $p<0.02$. Analysis of simple effects indicated that all groups displayed higher mean and peak firing rate during the first object trial and test trials (MFR: Hab xT1: $Zw=1.73$, $p<0.04$; T3 x Test: $Zw=3.16$, $p<0.04$; PFR: Hab xT1: $Zw=2.08$, $p<0.02$; T3 x Test: $Zw=0.96$, $p<0.05$]. No differences were observed in out-of- field firing rate. F-H) There were no differences during training or testing in other place cell parameters, including number of fields (F), field size (G), and spatial information content (H, $p>0.05$). Hab: habituation, T1-T3: training trials. YC: young control, YSD: young sleep deprived, OC: old control, OSD: old sleep deprived. Asterisks (*) represent significance using alpha=0.05. Statistical details in Data S1.

Estimation of remapping threshold

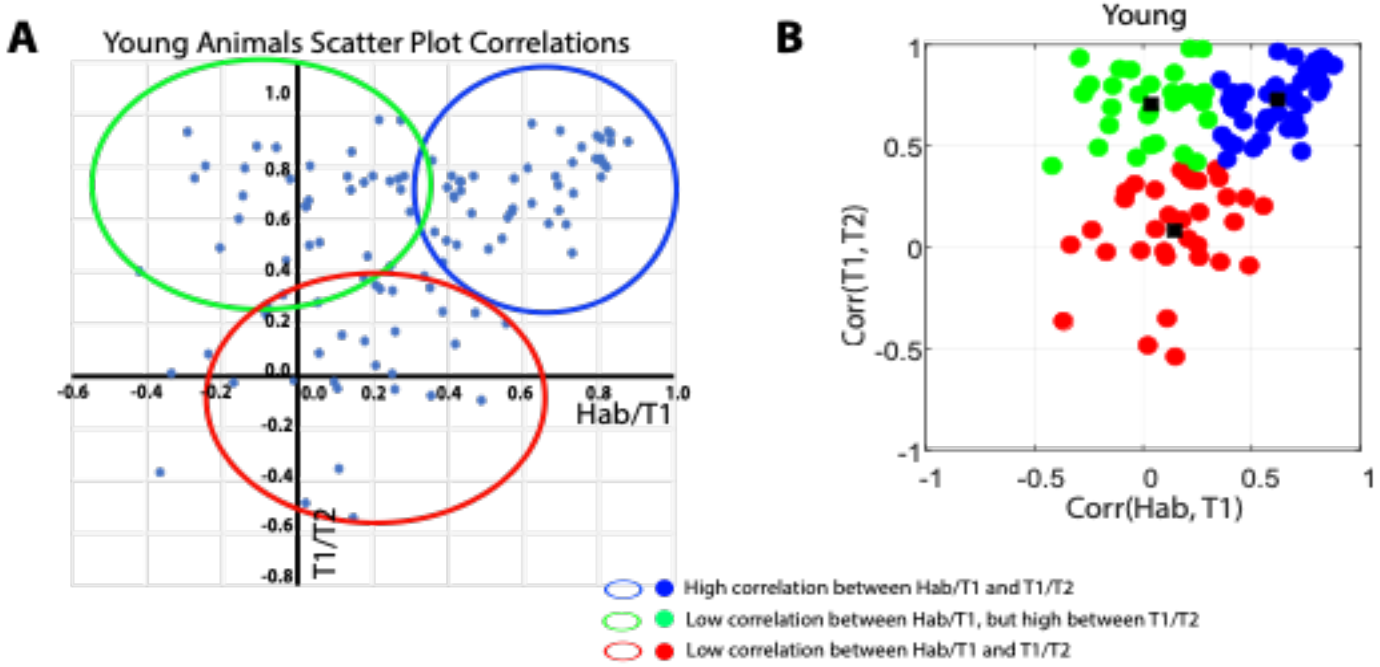

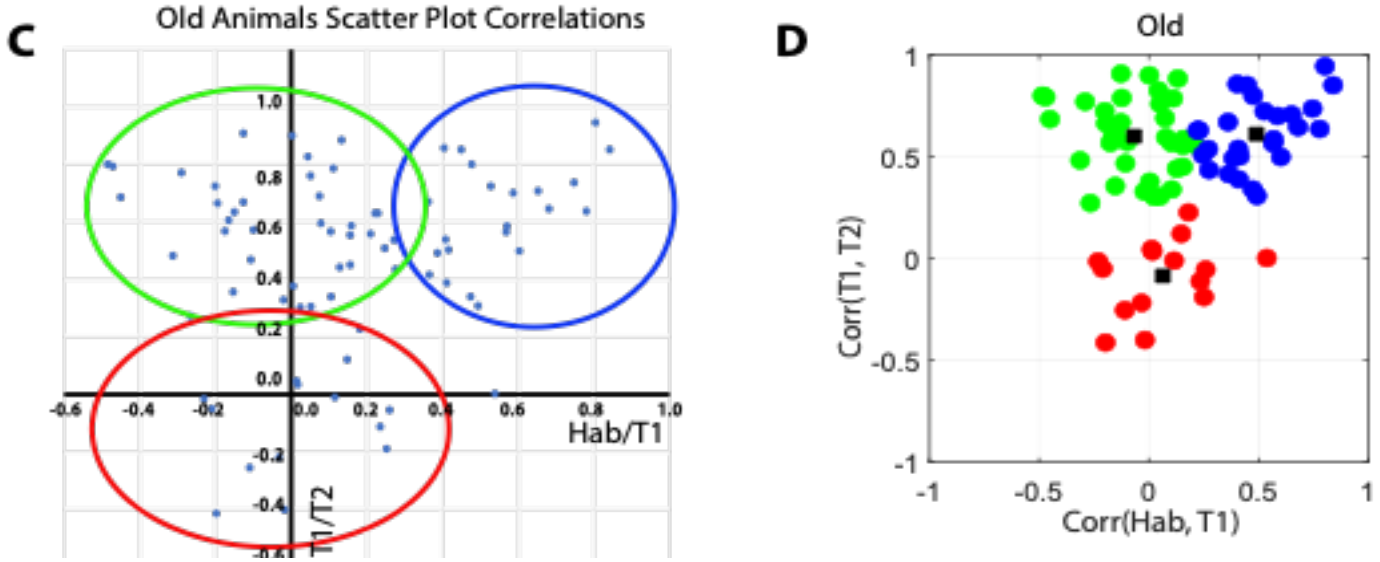

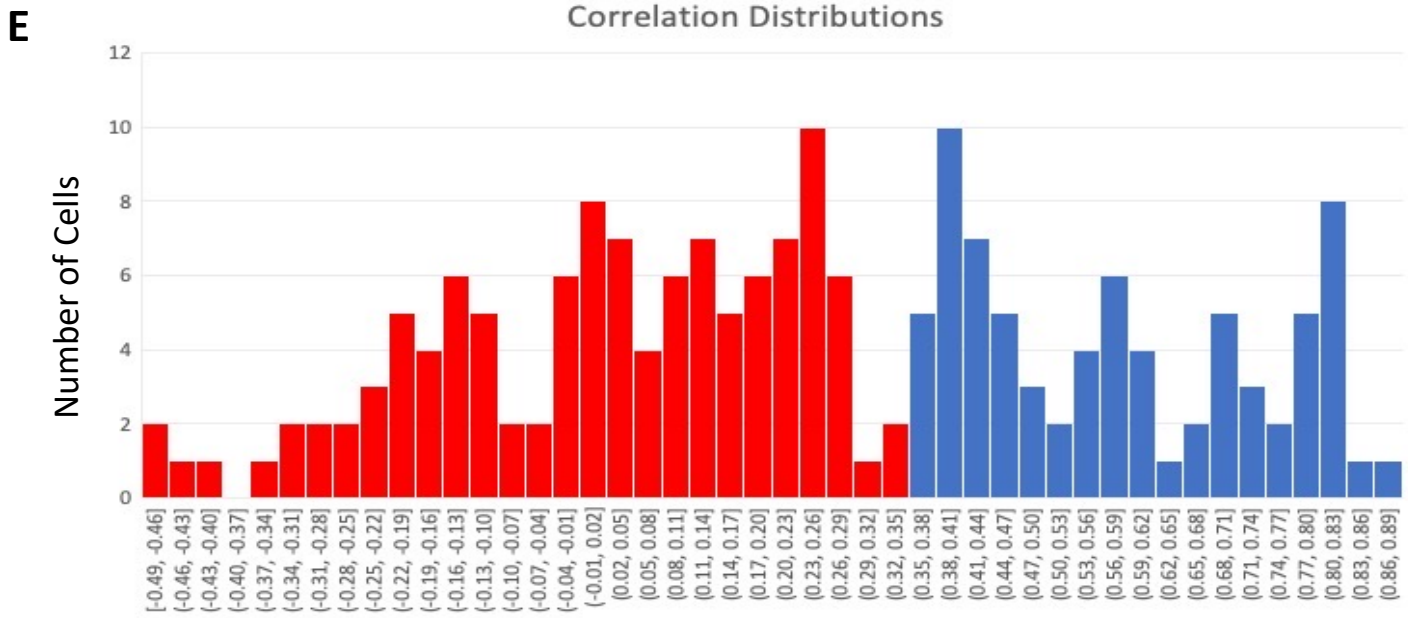

Figure S3

Figure S3, related to Figures 2E–F, 3, and 4. Estimation of remapping threshold. A-B) Scatter plots showing correlations between Hab/T1 and T1/T2 in young (A) and old (C) animals. B,D) Results of a machine learning algorithm, MATLAB *kmeans*, used to approximate the threshold to determine stability. The algorithm was instructed to group the data into 3 categories using correlation values from young (B) and old (D) mice. Means for each category are indicated by black squares. In both graphs the best approximation coincided with a threshold value of 0.35. Blue ellipse or dots contain correlation values displaying high stability between Hab/T1 and T1/T2, coinciding with our definition of context cells, green ellipse or dots contain correlation values displaying low stability between Hab/T1, but high stability between T1/T2, coinciding with our definition of object configuration cells, red ellipse or dots contain correlation values displaying low stability between Hab/T1 and T1/T2, coinciding with our definition of unstable cells. E) Histogram showing cell counts for all correlations between Hab and T1. Low stability cells are shown in red, whereas high stability cells are shown in blue. Note that the distributions are not normal, which justified the selection of robust statistics for all the analyses. Data in scatter plots and histogram distributions, as well as the output of a machine learning algorithm converge to indicate that the threshold of 0.35 is the best value to categorize cell types. Hab: habituation, T1-3: Trials1-3.

L-Ratio for clusters included in the unmoved control task.

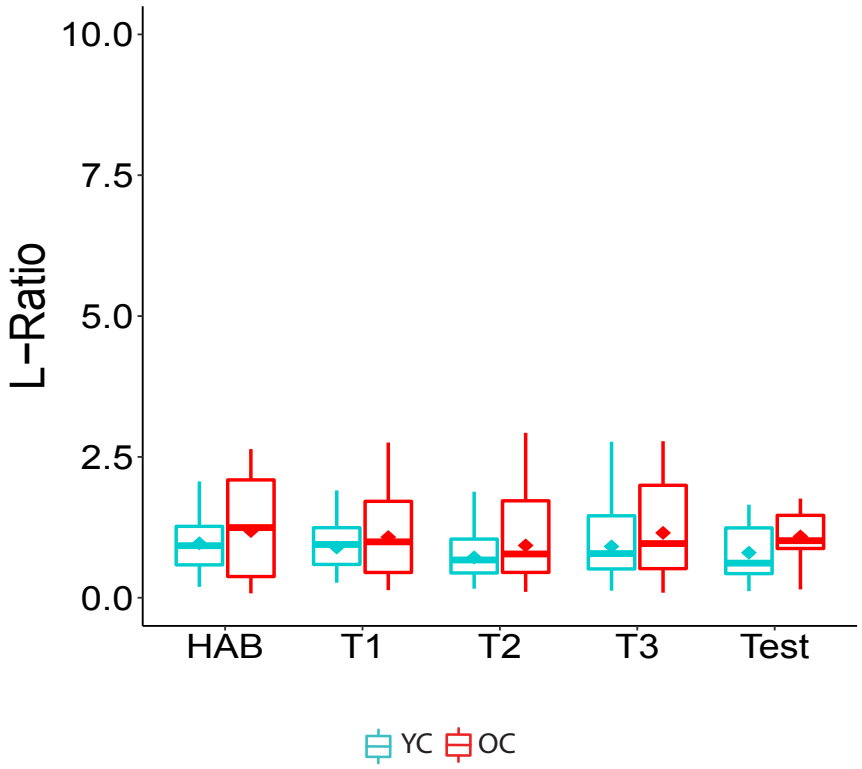

Figure S4, related to Figure 4. L-Ratio for clusters included in the unmoved control task. There were no differences between young and old controls in cluster quality across trials [effect of age: Fw(1)=1.14, p=0.30, effect of trial: Fw(4)=1.86, p=0.15; interaction Age * Trial: Fw(4)=0.07, p=0.99]. YC: young control, OC: old control. Statistical details in Data S1.

Validation of Bayes classifier

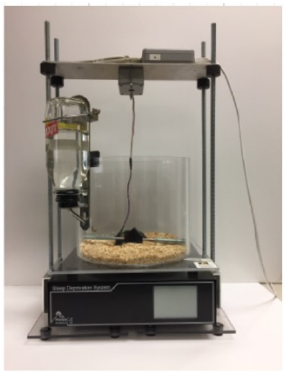

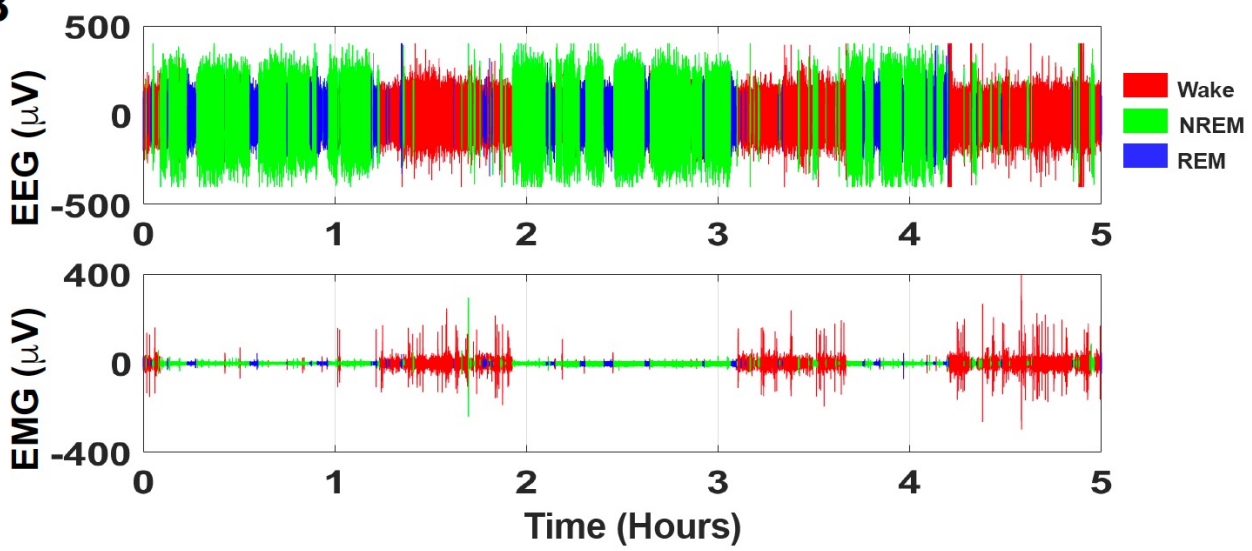

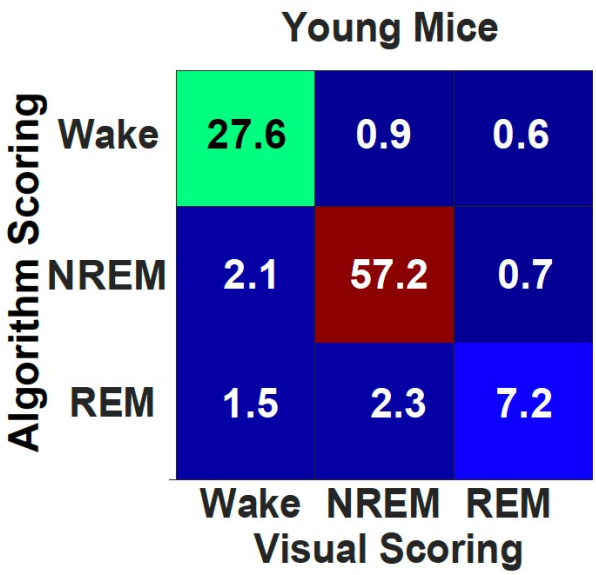

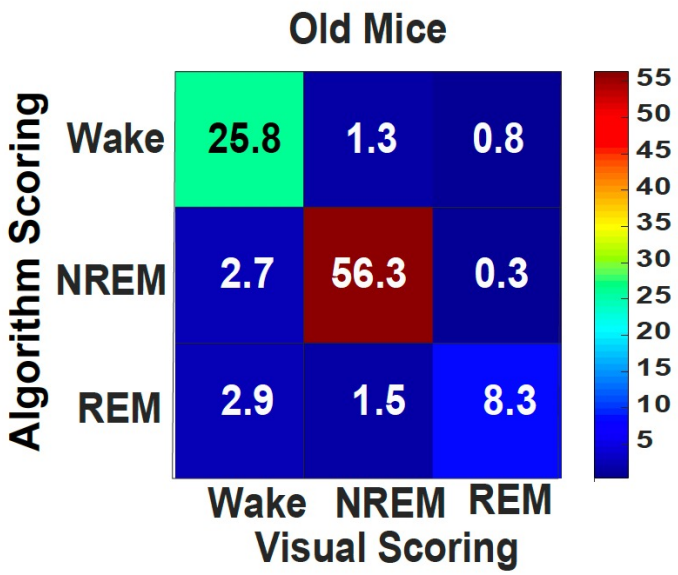

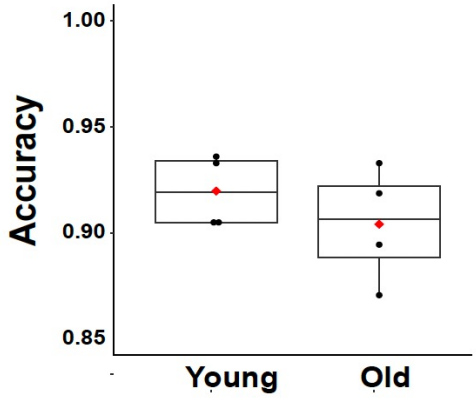

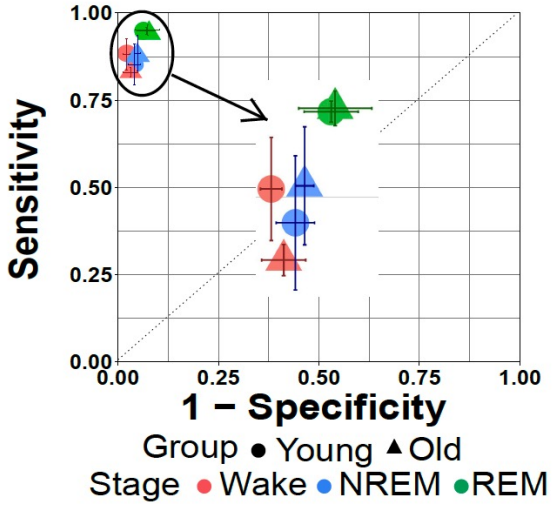

Figure S5

Figure S5, related to Figure 5A-F. Validation of Bayes classifier. A) Photograph of the SD chamber. B) Representative 5 hr sleep recording showing electroencephalogram (EEG, top panel) and electromyograph (EMG, bottom panel) color-coded using the output of a Bayes classifier. The color-coded EEG and EMG trace illustrates the accuracy of the classifier detecting Wake, NREM and REM periods. C-D) Average normalized confusion matrices for young (C) and old (D) mice. To determine the accuracy, sensitivity and specificity of the classifier, a confusion matrix was created by comparing visual and algorithm scored data in 4 young and 4 old mice. The results of this comparison were summed into the matrix for each animal. Each entry was then divided by the total number of epochs and multiplied by 100 to turn the values into percentages. Average confusion matrices were computed for young (C) and old (D) mice. E) Accuracy of the Bayes classifier for young and old mice. F) Receiver operating characteristic (ROC) curve showing average values of sensitivity (true positive rates) against false positive rates (1-specificity) for Wake, NREM, and REM in young and old mice. In the center of Figure F there is an enlargement of the execution data. The high accuracy of the classifier is illustrated by the fact that all values are in the upper left area, indicating high sensitivity and low fallout errors.

NREM and REM power spectra and relative sigma (RSP) and beta (RBP) power

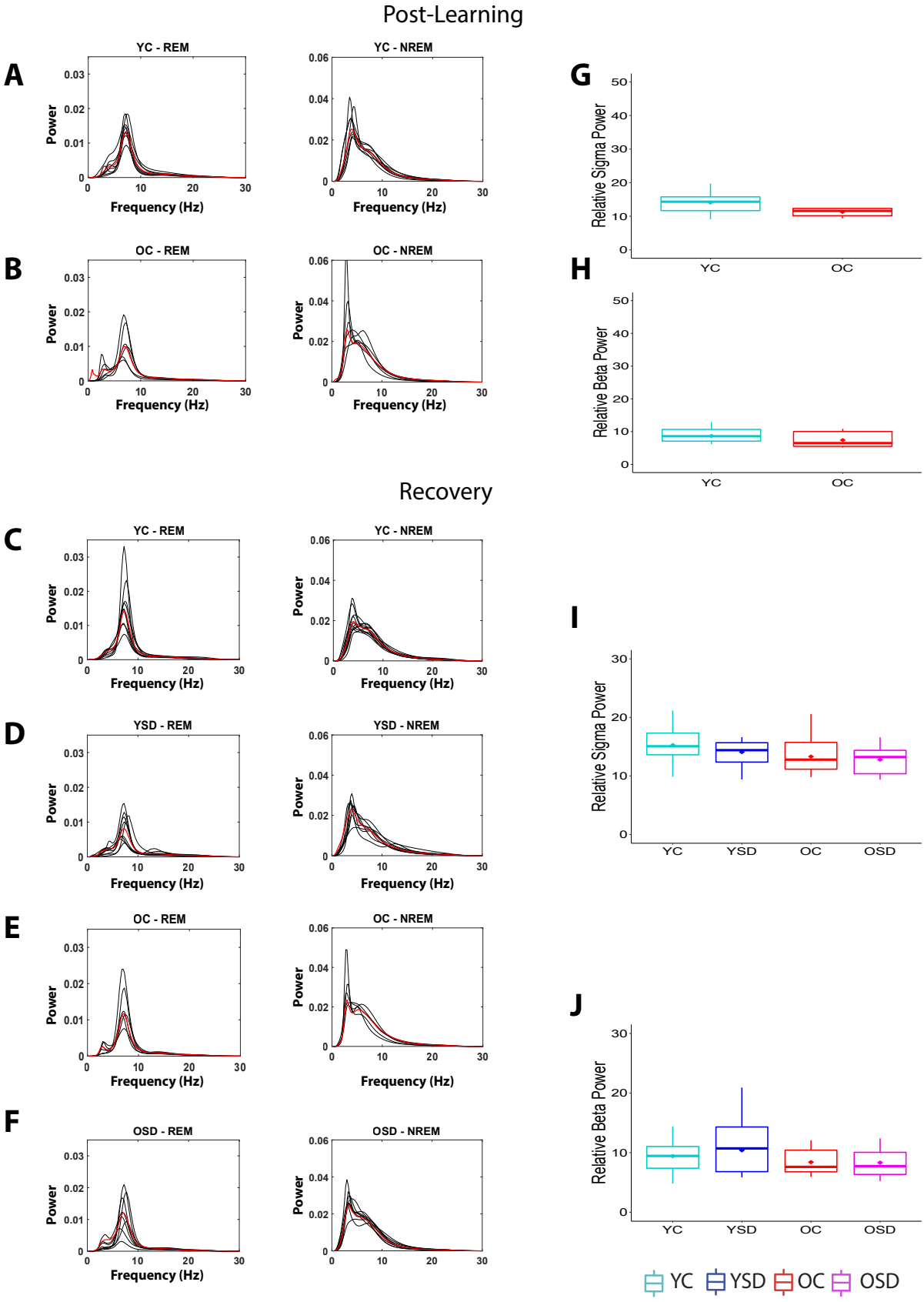

Figure S6, related to Figure 5G-N. NREM and REM power spectra and relative sigma (RSP) and beta (RBP) power. A-F) NREM and REM average (red) and individual (gray) power spectra during post-learning (A-B) and recovery (C-F) for all groups. G-J) Relative sigma (RSP) and beta (RBP) did not show differences during post-learning (G-H) or recovery (I-J). Sigma: 10-15 Hz, beta: 15-25 Hz. YC: young control, YSD: young sleep deprived, OC: old control, OSD: old sleep deprived. Statistical details in Data S1.